Single-RF Multi-User Communication Through Reconfigurable Intelligent Surfaces: An Information-Theoretic Analysis

Roy Karasik*, Osvaldo Simeone†, Marco Di Renzo‡, and Shlomo Shamai (Shitz)*
*Department of Electrical and Computer Engineering, Technion, Haifa 32000, Israel
†Centre for Telecommunications Research, Department of Informatics, King's College London, London WC2R 2LS, U.K.
‡Université Paris-Saclay, CNRS, CentraleSupélec, Laboratoire des Signaux et Systèmes, 91192 Gif-sur-Yvette, France
{royk@campus.technion.ac.il, osvaldo.simeone@kcl.ac.uk, marco.di-renzo@universite-paris-saclay.fr, sshlomo@ee.technion.ac.il}

2021 IEEE International Symposium on Information Theory (ISIT) | 978-1-5386-8209-8/21/$31.00 ©2021 IEEE | DOI: 10.1109/ISIT45174.2021.9518055

***Abstract*—Reconfigurable intelligent surfaces (RISs) are typically used in multi-user systems to mitigate interference among active transmitters. In contrast, this paper studies a setting with a conventional active encoder as well as a passive encoder that modulates the reflection pattern of the RIS. The RIS hence serves the dual purpose of improving the rate of the active encoder and of enabling communication from the second encoder. The capacity region is characterized, and information-theoretic insights regarding the trade-offs between the rates of the two encoders are derived by focusing on the high- and low-power regimes.**

I. Introduction

A reconfigurable intelligent surface (RIS) is a nearly-passive device that can shape the wireless propagation channel by applying phase shifts to the incident signals [1]–[7]. In multi-user (MU) systems, RISs can help mitigate inter-user interference and obtain beamforming gain for standard active transmitters [8]–[15]. To this end, the configuration of the RIS is kept fixed for the duration of a coherence interval and optimized to maximize some function of the achievable rates [8]–[15]. In this paper, we study a different use of RISs, whereby a single active transmitter coexists with a *passive* user, having no direct radio frequency (RF) chain, that conveys its own message by modulating the reflection pattern of the RIS (see Fig. 1). With reference to Fig. 1, the RIS is accordingly used for the dual purpose of enhancing the rate of the active encoder (Encoder 1) and of enabling communication for the passive encoder (Encoder 2). Unlike prior work [16] that focused on a specific transmission strategy, this paper concentrates on the information-theoretic analysis of the rate trade-offs between the two encoders, providing fundamental insights.

Related Work: A comprehensive survey of the state-of-the-art on RIS-aided MU systems is available in [1]. As notable representative examples of works involving active transmitters, the maximization of the weighted sum-rate in RIS-aided MU systems was studied in [8]–[11], whereas references [12], [13] focused on optimizing the energy efficiency, and papers [14], [15] on physical-layer security and outage-probability enhancements. A MU system with an active transmitter and a passive encoder, akin to Fig. 1, was proposed in [16] by assuming binary modulation, a single receiver antenna, and a specific successive interference cancellation decoding strategy.

This work has been supported by the European Research Council (ERC) and by the Information and Communication Technologies (ICT) under the European Union's Horizon 2020 Research and Innovation Programme (Grant Agreement Nos. 694630, 725731, and 871464).

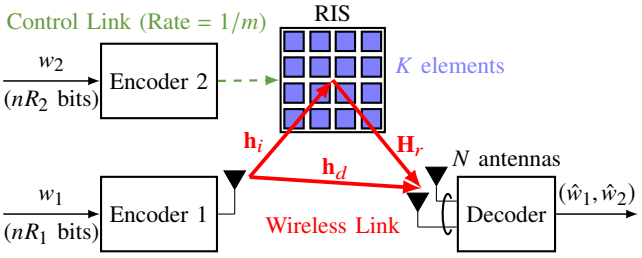

Fig. 1. In the system under study, Encoder 1 is active and it encodes its message w_1 into a codeword of n symbols sent on the wireless link; whereas Encoder 2 is passive and it encodes the message w_2 into a control action, which is sent on the control link to the RIS at a rate of one action every m channel symbols.

From an information-theoretic perspective, the single-RF MU communication system depicted in Fig. 1 can be viewed as a multiple access channel (MAC) with both multiplicative and additive elements. The capacity of the Gaussian multiplicative MAC was derived in [17] for two active encoders. The capacity region of a backscatter multiplicative MAC, which can be viewed as a special case of the RIS-aided MU communication system in Fig. 1 with one reflecting element, was studied in [18]. Under the assumptions of a single receiver antenna and Gaussian codebooks, this work shows that conventional time-sharing schemes are suboptimal in the high-power and weak-backscatter regimes. The capacity of an RIS-aided *single-user* channel was derived in [19].

Main Contributions: In this paper, we study the RIS-aided MU system illustrated in Fig. 1, in which Encoder 1 is active, whereas Encoder 2 can only alter the reflection pattern of the RIS in a passive manner. We derive the capacity region under the practical assumptions of a multi-antenna decoder, a finite-input constellation, and a set of discrete phase shifts at the RIS. Then, we specialize the results for the high- and low-power regimes, showing that: *(i)* for sufficiently high transmission power, both encoders can simultaneously communicate at maximum rate; and *(ii)* in the low-power regime, Encoder 1 can achieve maximum rate if and only if Encoder 2 does not communicate, while Encoder 2 can achieve its maximum rate

while still enabling non-zero-rate communication for Encoder 1. Finally, numerical examples demonstrate the dual role of the RIS as means to enhance the transmitted signal on the one hand and as the enabler of MU communication on the other hand.

Notation: Random variables, vectors, and matrices are denoted by lowercase, boldface lowercase, and boldface uppercase Roman-font letters, respectively. Realizations of random variables, vectors, and matrices are denoted by lowercase, boldface lowercase, and boldface uppercase italic-font letters, respectively. For example, x is a realization of random variable x, $\boldsymbol{x}$ is a realization of random vector $\mathbf{x}$, and $\boldsymbol{X}$ is a realization of random matrix $\mathbf{X}$. For any positive integer K, we define the set $[K] \triangleq \{1, 2, \ldots, K\}$. The cardinality of a set $\mathcal{A}$ is denoted as $|\mathcal{A}|$. The ℓ^2-norm and the conjugate transpose of a vector $\boldsymbol{v}$ are denoted as $\|\boldsymbol{v}\|$ and $\boldsymbol{v}^*$, respectively. $\mathrm{diag}(\boldsymbol{x})$ represents a diagonal matrix with diagonal given by the vector $\boldsymbol{x}$. The vectorization of matrix $\boldsymbol{H}$, i.e., the operator that stacks the columns of $\boldsymbol{H}$ on top of one another, is denoted by $\mathrm{vec}(\boldsymbol{H})$. The Kronecker product $\boldsymbol{I}_m \otimes \boldsymbol{B}$ of the identity matrix of size m and matrix $\boldsymbol{B}$ is denoted as $\boldsymbol{B}^{m\otimes}$.

II. System Model

We consider the system depicted in Fig. 1 in which two encoders communicate with a decoder equipped with N antennas over a quasi-static fading channel in the presence of an RIS that comprises K nearly-passive reconfigurable elements. Encoder 1 is equipped with a single-RF transmitter and encodes its message $w_1 \in [2^{nR_1}]$ of rate R_1 [bits/symbol] into a codeword of n symbols sent on the wireless link to the decoder. In contrast, Encoder 2 encodes its message $w_2 \in [2^{nR_2}]$ of rate R_2 [bits/symbol] in a passive manner by modulating the reflection pattern of the RIS. The reflection pattern is controlled through a rate-limited control link, and is defined by the phase shifts that each of the K RIS elements applies to the impinging wireless signal. Encoder 2 represents, for example, a sensor embedded in the RIS that applies metasurface-based modulation in order to convey its sensed data without emitting a new radio wave [5, Sec. 3.3].

A coding slot consists of n symbols, which are divided into n/m blocks of m symbols each, with n/m assumed to be integer. Specifically, the codeword transmitted by Encoder 1 as a function of message w_1 occupies the entire coding slot, and it includes n symbols from a constellation $\mathcal{S}$ of $S = |\mathcal{S}|$ points. Furthermore, the RIS is controlled by Encoder 2 by selecting the phase shift applied by each of the K elements of the RIS from a finite set $\mathcal{A}$ of $A = |\mathcal{A}|$ distinct hardware-determined values as a function of the message w_2. Due to practical limitations on the RIS control rate, the phase shifts can only be modified once for each block of m consecutive transmitted symbols. During the tth block, the fraction of the codeword of Encoder 1 consisting of m transmitted symbols is denoted by $\mathbf{s}(t) = (\mathrm{s}_1(t), \ldots, \mathrm{s}_m(t))^{\mathsf{T}} \in \mathcal{S}^{m\times 1}$, and is assumed to satisfy the power constraint $\mathbb{E}[\mathbf{s}^*(t)\mathbf{s}(t)] \leq m$. The phase shifts applied by the RIS in the tth block are denoted by the vector

$$e^{j\boldsymbol{\theta}(t)} \triangleq (e^{j\theta_1(t)}, \ldots, e^{j\theta_K(t)})^{\mathsf{T}}, \tag{1}$$

with $\theta_k(t) \in \mathcal{A}$ being the phase shift applied by the kth RIS element, $k \in [K]$.

We assume quasi-static flat-fading wireless channels, which remain fixed throughout a coding slot. Specifically, the channel from Encoder 1 to the decoder is denoted by vector $\mathbf{h}_d \in \mathbb{C}^{M\times 1}$; the channel from Encoder 1 to the RIS is denoted by the vector $\mathbf{h}_i \in \mathbb{C}^{K\times 1}$; and the channel from the RIS to the N receiving antennas is denoted by the matrix $\mathbf{H}_r \in \mathbb{C}^{N\times K}$. Furthermore, we assume that $\mathbf{h}_d$, $\mathbf{h}_i$, and $\mathbf{H}_r$ are drawn from a continuous distribution. Finally, we denote the signal received by the N antennas for the qth transmitted symbol in block $t \in [n/m]$ by $\mathbf{y}_q(t) \in \mathbb{C}^{N\times 1}$, $q \in [m]$. The overall received signal matrix $\mathbf{Y}(t) = (\mathbf{y}_1(t), \ldots, \mathbf{y}_m(t)) \in \mathbb{C}^{N\times m}$ in the tth sub-block can hence be written as

$$\begin{aligned}\mathbf{Y}(t) &= \sqrt{P}\mathbf{H}_r \,\mathrm{diag}\left(e^{j\boldsymbol{\theta}(t)}\right)\mathbf{h}_i\mathbf{s}^{\mathsf{T}}(t) + \mathbf{h}_d\mathbf{s}^{\mathsf{T}}(t) + \mathbf{Z}(t)\\ &= \sqrt{P}\left(\mathbf{H}_{ri}e^{j\boldsymbol{\theta}(t)} + \mathbf{h}_d\right)\mathbf{s}^{\mathsf{T}}(t) + \mathbf{Z}(t),\end{aligned} \tag{2}$$

where $P > 0$ denotes the transmission power of Encoder 1; the matrix $\mathbf{H}_{ri} \triangleq \mathbf{H}_r\,\mathrm{diag}(\mathbf{h}_i) \in \mathbb{C}^{N\times K}$, combines the channels $\mathbf{h}_i$ and $\mathbf{H}_r$; and the matrix $\mathbf{Z}(t) \in \mathbb{C}^{N\times m}$, whose elements are independent and identically distributed (i.i.d.) as $\mathcal{CN}(0,1)$, denotes the additive white Gaussian noise at the receiving antennas. In order to characterize the distribution of the output signal $\mathbf{Y}(t)$ in (2), we vectorize it as

$$\mathbf{y}(t) \triangleq \mathrm{vec}(\mathbf{Y}(t)) = \sqrt{P}\left(\mathbf{H}_{ri}e^{j\boldsymbol{\theta}(t)} + \mathbf{h}_d\right)^{m\otimes}\mathbf{s}(t) + \mathbf{z}(t), \tag{3}$$

where we have defined the vector $\mathbf{z}(t) \triangleq \mathrm{vec}(\mathbf{Z}(t)) \in \mathbb{C}^{Nm\times 1}$.

We assume that both the encoders and the decoder have perfect channel state information (CSI), in the sense that the channel matrix $\mathbf{H}_{ri}$ and channel vector $\mathbf{h}_d$ are known. Having received signal $\mathbf{y}(t)$ in (3) for $t \in [n/m]$, the decoder produces the estimates $\hat{w}_\ell = \hat{w}_\ell(\mathbf{y}(1), \ldots, \mathbf{y}(n/m), \mathbf{H}_{ri}, \mathbf{h}_d)$, for $\ell = 1, 2$, using knowledge of the CSI. Given channel realizations $\boldsymbol{H}_{ri}$ and $\boldsymbol{h}_d$, a rate pair $(R_1(\boldsymbol{H}_{ri}, \boldsymbol{h}_d), R_2(\boldsymbol{H}_{ri}, \boldsymbol{h}_d))$ is said to be *achievable* if the probability of error satisfies the limit $\Pr(\hat{w}_1 \neq w_1, \hat{w}_2 \neq w_2) \to 0$ when the codeword length grows large, i.e., $n \to \infty$. The corresponding capacity region $\mathcal{C}(\boldsymbol{H}_{ri}, \boldsymbol{h}_d)$ is defined as the closure of the set of achievable rate pairs.

III. Capacity Region

In this section, we first derive a general characterization of the capacity region $\mathcal{C}(\boldsymbol{H}_{ri}, \boldsymbol{h}_d)$ for the channel in (3). Then, we leverage this result to provide theoretical insights into the trade-offs between the rate of the two encoders in Fig. 1 by focusing on the low- and high-power regimes.

Most existing works on the multiplicative Gaussian MAC [17], [18] and on RIS-aided systems (see, e.g., [8]) consider Gaussian codebooks for the transmitted signal $\mathbf{s}(t)$. This implies that the resulting achievable rates are formulated in the standard form "$\log_2(1 + \mathrm{SNR})$". In contrast, as described in Section II, we focus our attention on the more practical model in which the transmitted symbols and the RIS elements' phase response take values from finite sets [20]. Therefore, in a manner similar to [19], the expressions for the achievable rates that we present in this section are more complex, and require the following definition.

Definition 1: The cumulant-generating function (CGF) of a random variable u conditioned on a random vector $\mathbf{x}$ is defined as

$$\kappa_r(\mathrm{u}|\mathbf{x}) \triangleq \mathbb{E}\left[\log_2\left(\mathbb{E}\left[e^{r\mathrm{u}}|\mathbf{x}\right]\right)\right], \quad \text{for } r \in \mathbb{R}, \tag{4}$$

and the value of the conditional CGF for $r = 1$ is denoted as $\kappa(\mathrm{u}|\mathbf{x}) \triangleq \kappa_1(\mathrm{u}|\mathbf{x})$.

We now characterize the capacity region in the form of a union of rate regions, with each region corresponding to rates achievable for a specific choice of encoding distributions $p_{\mathbf{s}}(\boldsymbol{s})$ and $p_{\boldsymbol{\theta}}(\boldsymbol{\theta})$ of the transmitted symbols $\mathbf{s}(t)$ and RIS phase shifts $\boldsymbol{\theta}(t)$ in (3), respectively.

Proposition 1: For input distributions $p_{\mathbf{s}}(\boldsymbol{s})$ and $p_{\boldsymbol{\theta}}(\boldsymbol{\theta})$, let $\mathcal{R}(p_{\mathbf{s}}, p_{\boldsymbol{\theta}}, \boldsymbol{H}_{ri}, \boldsymbol{h}_d)$ be the set of rate pairs $(R_1(\boldsymbol{H}_{ri}, \boldsymbol{h}_d), R_2(\boldsymbol{H}_{ri}, \boldsymbol{h}_d))$ such that the inequalities

$$R_\ell(\boldsymbol{H}_{ri}, \boldsymbol{h}_d) \le -N\log_2(e) - \frac{1}{m}\kappa(\mathrm{u}_\ell|\mathbf{s}_1, \boldsymbol{\theta}_1, \mathbf{z}), \quad \ell \in \{1,2\}, \tag{5a}$$

and

$$R_1(\boldsymbol{H}_{ri}, \boldsymbol{h}_d) + R_2(\boldsymbol{H}_{ri}, \boldsymbol{h}_d) \le -N\log_2(e) - \frac{1}{m}\kappa(\mathrm{u}_3|\mathbf{s}_1, \boldsymbol{\theta}_1, \mathbf{z}) \tag{5b}$$

hold, where random variable u_1, u_2, and u_3 are defined as

$$\mathrm{u}_1 \triangleq -\left\|\mathbf{z} + \sqrt{P}\left(\boldsymbol{H}_{ri}e^{j\boldsymbol{\theta}_1} + \boldsymbol{h}_d\right)^{m\otimes}(\mathbf{s}_1 - \mathbf{s}_2)\right\|^2, \tag{6a}$$

$$\mathrm{u}_2 \triangleq -\left\|\mathbf{z} + \sqrt{P}\left(\boldsymbol{H}_{ri}\left[e^{j\boldsymbol{\theta}_1} - e^{j\boldsymbol{\theta}_2}\right]\right)^{m\otimes}\mathbf{s}_1\right\|^2, \tag{6b}$$

$$\mathrm{u}_3 \triangleq -\left\|\mathbf{z} + \sqrt{P}\left(\boldsymbol{H}_{ri}e^{j\boldsymbol{\theta}_1} + \boldsymbol{h}_d\right)^{m\otimes}\mathbf{s}_1 - \sqrt{P}\left(\boldsymbol{H}_{ri}e^{j\boldsymbol{\theta}_2} + \boldsymbol{h}_d\right)^{m\otimes}\mathbf{s}_2\right\|^2, \tag{6c}$$

respectively, with independent random vectors $\mathbf{s}_1, \mathbf{s}_2 \sim p_{\mathbf{s}}(\boldsymbol{s})$, $\boldsymbol{\theta}_1, \boldsymbol{\theta}_2 \sim p_{\boldsymbol{\theta}}(\boldsymbol{\theta})$, and $\mathbf{z} \sim \mathcal{CN}(\mathbf{0}, \boldsymbol{I}_{Nm})$. The capacity region $\mathcal{C}(\boldsymbol{H}_{ri}, \boldsymbol{h}_d)$ is the convex hull of the union of the regions $\mathcal{R}(p_{\mathbf{s}}, p_{\boldsymbol{\theta}}, \boldsymbol{H}_{ri}, \boldsymbol{h}_d)$ over all input distributions $p_{\mathbf{s}}(\boldsymbol{s})$ and $p_{\boldsymbol{\theta}}(\boldsymbol{\theta})$ with $\boldsymbol{s} \in \mathcal{S}^{m\times 1}$, $\boldsymbol{\theta} \in \mathcal{A}^{K\times 1}$, such that $\mathbb{E}[\mathbf{s}^*\mathbf{s}] \le m$.

Proof: See Appendix A. ∎

Next, we specialize the results in Proposition 1 to characterize the capacity region in the high- and low-power regimes.

A. High-Power Regime

The following corollary shows that the capacity region $\mathcal{C}(\boldsymbol{H}_{ri}, \boldsymbol{h}_d)$ converges to a rectangle as the power of Encoder 1 increases.

Corollary 1: For any finite constellation $\mathcal{S}$ of $S = |\mathcal{S}|$ points and any set $\mathcal{A}$ of $A = |\mathcal{A}|$ phases, let $\overline{\mathcal{C}}$ be the set of rate pairs (R_1, R_2) such that

$$\overline{\mathcal{C}} \triangleq \left\{(R_1, R_2) : R_1 \le \log_2(S),\ R_2 \le \frac{K}{m}\log_2(A)\right\}. \tag{7}$$

The capacity region $\mathcal{C}(\boldsymbol{H}_{ri}, \boldsymbol{h}_d)$ converges to $\overline{\mathcal{C}}$ as the power P increases in the sense that $\mathcal{C}(\boldsymbol{H}_{ri}, \boldsymbol{h}_d) \subseteq \overline{\mathcal{C}}$, and there exists a sequence of achievable rate pairs $(R_1(\boldsymbol{H}_{ri}, \boldsymbol{h}_d), R_2(\boldsymbol{H}_{ri}, \boldsymbol{h}_d)) \in \mathcal{C}(\boldsymbol{H}_{ri}, \boldsymbol{h}_d)$ such that, almost surely,

$$\lim_{P\to\infty} R_1(\boldsymbol{H}_{ri}, \boldsymbol{h}_d) = \log_2(S), \tag{8a}$$

$$\lim_{P\to\infty} R_2(\boldsymbol{H}_{ri}, \boldsymbol{h}_d) = \frac{K}{m}\log_2(A). \tag{8b}$$

Proof: See Appendix B. ∎

Corollary 1 implies that, for sufficiently high power P, both encoders can simultaneously achieve their maximum rates. As a result, while not useful in increasing the high-power rate of Encoder 1, the presence of the RIS enables communication at the maximum rate for Encoder 2 without creating deleterious interference on Encoder 1's transmission.

B. Low-Power Regime

In this section, we characterize the capacity region $\mathcal{C}(\boldsymbol{H}_{ri}, \boldsymbol{h}_d)$ in the low-power regime. To simplify the analysis, we focus on a system with one receiver antenna, $N = 1$, and an RIS control ratio of $m = 1$. For this special case, the channel (3) can be written as

$$\mathrm{y}(t) = \sqrt{P}\left(\mathbf{h}_{ri}^{\mathsf{T}}e^{j\boldsymbol{\theta}(t)} + \mathrm{h}_d\right)\mathrm{s}(t) + \mathrm{z}(t), \tag{9}$$

where $\mathbf{h}_{ri} \in \mathbb{C}^{K\times 1}$ and $\mathrm{h}_d \in \mathbb{C}$ denote the reflected and direct channel paths, respectively, and $\mathrm{z}(t) \sim \mathcal{CN}(0,1)$ denotes the additive white Gaussian noise. Furthermore, we assume that the phase shift applied by each element of the RIS is chosen from a finite set of A uniformly spaced phases, i.e., $\mathcal{A} = \{0, 2\pi/A, \ldots, 2\pi(A-1)/A\}$; and that $\mathcal{S}$ is a zero-mean input constellation, i.e., $\sum_{s\in\mathcal{S}} s = 0$, which is known to achieve the minimum energy per bit in many single-user channels [21]–[23].

In order to formulate the capacity region in the low-power regime, we define the normalized rate $r_\ell(\boldsymbol{h}_{ri}, h_d)$, $\ell \in \{1,2\}$, for unit of power as

$$r_\ell(\boldsymbol{h}_{ri}, h_d) \triangleq \lim_{P\to 0}\frac{R_\ell(\boldsymbol{h}_{ri}, h_d)}{P}. \tag{10}$$

The capacity region in the low-power regime $\underline{\mathcal{C}}(\boldsymbol{h}_{ri}, h_d)$ is accordingly defined as the closure of the set of achievable normalized rate pairs (see, e.g., [24]).

Proposition 2: For input distributions $p_{\mathrm{s}}(s)$ and $p_{\boldsymbol{\theta}}(\boldsymbol{\theta})$, let $\underline{\mathcal{R}}(p_{\mathrm{s}}, p_{\boldsymbol{\theta}}, \boldsymbol{h}_{ri}, h_d)$ be the set of normalized rate pairs $(r_1(\boldsymbol{h}_{ri}, h_d), r_2(\boldsymbol{h}_{ri}, h_d))$ such that the inequalities

$$r_\ell(\boldsymbol{h}_{ri}, h_d) \le \frac{\mathbb{E}[\underline{\mathrm{u}}_\ell]}{\ln(2)}, \quad \ell \in \{1,2\}, \tag{11a}$$

$$\text{and } r_1(\boldsymbol{h}_{ri}, h_d) + r_2(\boldsymbol{h}_{ri}, h_d) \le \frac{\mathbb{E}[\underline{\mathrm{u}}_3]}{\ln(2)} \tag{11b}$$

hold, where random variable $\underline{\mathrm{u}}_1$, $\underline{\mathrm{u}}_2$, and $\underline{\mathrm{u}}_3$ are defined as

$$\underline{\mathrm{u}}_1 \triangleq \left|\left(\boldsymbol{h}_{ri}^{\mathsf{T}}e^{j\boldsymbol{\theta}_1} + h_d\right)(\mathrm{s}_1 - \mathrm{s}_2)\right|^2, \tag{12a}$$

$$\underline{\mathrm{u}}_2 \triangleq \left|\boldsymbol{h}_{ri}^{\mathsf{T}}\left(e^{j\boldsymbol{\theta}_1} - e^{j\boldsymbol{\theta}_2}\right)\mathrm{s}_1\right|^2, \tag{12b}$$

$$\underline{\mathrm{u}}_3 \triangleq \left|\left(\boldsymbol{h}_{ri}^{\mathsf{T}}e^{j\boldsymbol{\theta}_1} + h_d\right)\mathrm{s}_1 - \left(\boldsymbol{h}_{ri}^{\mathsf{T}}e^{j\boldsymbol{\theta}_2} + h_d\right)\mathrm{s}_2\right|^2, \tag{12c}$$

respectively, with independent random variables $\mathrm{s}_1, \mathrm{s}_2 \sim p_{\mathrm{s}}(s)$ and random vectors $\boldsymbol{\theta}_1, \boldsymbol{\theta}_2 \sim p_{\boldsymbol{\theta}}(\boldsymbol{\theta})$. The capacity region in the low-power regime $\underline{\mathcal{C}}(\boldsymbol{h}_{ri}, h_d)$ is the convex hull of the union of the regions $\underline{\mathcal{R}}(p_{\mathrm{s}}, p_{\boldsymbol{\theta}}, \boldsymbol{h}_{ri}, h_d)$ over all input distributions $p_{\mathrm{s}}(s)$ and $p_{\boldsymbol{\theta}}(\boldsymbol{\theta})$ with $s \in \mathcal{S}$, $\boldsymbol{\theta} \in \mathcal{A}^{K\times 1}$, such that $\mathbb{E}[|\mathrm{s}|^2] \le 1$.

Proof: See Appendix C. ∎

Unlike the high-power regime, the low-power capacity region (11) is not a rectangle, implying that it is not possible for both encoders to communicate at their respective maximum rates. The next corollary elaborates on this point.

Corollary 2: Let $\tilde{\boldsymbol{\theta}}$ be the beamforming phase-shift vector maximizing Encoder 1's rate, i.e.,

$$\tilde{\boldsymbol{\theta}} \triangleq \arg\max_{\boldsymbol{\theta}\in\mathcal{A}^{K\times 1}}\left|\boldsymbol{h}_{ri}^{\mathsf{T}}e^{j\boldsymbol{\theta}} + h_d\right|^2. \tag{13}$$

In the low-power regime, Encoder 1 can achieve its maximum normalized rate

$$r_1(\boldsymbol{h}_{ri}, h_d) = \frac{2}{\ln(2)}\left|\boldsymbol{h}_{ri}^{\mathsf{T}}e^{j\tilde{\boldsymbol{\theta}}} + h_d\right|^2 \tag{14}$$

if and only if Encoder 2 does not communicate, i.e., $r_2(\boldsymbol{h}_{ri}, h_d) = 0$. In contrast, if $|\boldsymbol{h}_{ri}^{\mathsf{T}} e^{j\tilde{\boldsymbol{\theta}}} + h_d|^2 > \|\boldsymbol{h}_{ri}\|^2$, Encoder 2 can achieve its maximum normalized rate

$$r_2(\boldsymbol{h}_{ri}, h_d) = \frac{2}{\ln(2)} \|\boldsymbol{h}_{ri}\|^2, \tag{15}$$

while Encoder 1 communicates at a normalized rate of

$$r_1(\boldsymbol{h}_{ri}, h_d) = \frac{2}{\ln(2)} \left(\left| \boldsymbol{h}_{ri}^{\mathsf{T}} e^{j\tilde{\boldsymbol{\theta}}} + h_d \right|^2 - \|\boldsymbol{h}_{ri}\|^2 \right). \tag{16}$$

Proof: See Appendix D. ∎

The asymmetry between Encoder 1 and Encoder 2 revealed by Corollary 2 stems from the fact the, in order for Encoder 1 to obtain its maximum rate in the low-power regime, Encoder 2 needs to steer its phases according to the beamforming solution (13). This in turn makes it impossible to encode additional information for Encoder 2. In contrast, Encoder 2's maximum rate can be obtained as long as Encoder 1's signal is transmitted at the maximum power and can be decoded while treating the modulation of the RIS's phases by Encoder 2 as a nuisance.

We finally remark that Corollary 1 and Corollary 2 imply that time-sharing, which would yield a triangular rate region, is suboptimal in both high- and low-power regimes. This is in contrast to the multiplicative MAC studied in [17] that assumes two standard active encoders with separate power constraints.

IV. Examples

In this section, we provide numerical examples for the capacity region derived in Section III. For the phase response set, we consider A uniformly spaced phases in the set $\mathcal{A} = \{0, 2\pi/A, \ldots, 2\pi(A-1)/A\}$, whereas, for the input constellation, we consider amplitude shift keying (ASK) and phase-shift keying (PSK) modulations. In addition, we assume a channel vector $\boldsymbol{h}_d$ with elements having amplitude 1, and a channel matrix $\boldsymbol{H}_{ri}$ with elements having amplitude $\alpha > 0$, where α denotes the path-loss ratio between the reflected and direct paths. The phases of $\boldsymbol{H}_{ri}$ and $\boldsymbol{h}_d$ used in this section are summarized in Table I. Furthermore, the expectation over Gaussian random vectors, e.g., $\mathbf{z}$ in Proposition 1, is evaluated via a Monte Carlo empirical averages.

In Fig. 2, we plot the capacity region for an average power constraint of $P = -20$ dB, $N = 2$ receiver antennas, $K = 4$ RIS elements, $A = 2$ available phase shifts, a symbol-to-RIS control rate $m = 2$, input constellation given by BPSK, i.e., $\mathcal{S} = \{-1, 1\}$, and a path-loss ratio of $\alpha = 0.5$ or $\alpha = 1$. In addition, we plot for reference the maximum rate achievable by Encoder 1 for a channel with no RIS, i.e., for $\boldsymbol{H}_{ri} = \mathbf{0}$. By comparing with the capacity of the channel with no RIS, Fig. 2 illustrates the two roles of the RIS: The RIS can be used to increase the rate of Encoder 1 by beamforming the transmitted signal, and it can enable communication from a passive secondary user. In this regard, Fig. 2 demonstrates that the insights obtained in Corollary 2 by studying the low-power regime carry over to more general conditions. In particular, the maximum rate for Encoder 1 is achieved if and only if Encoder 2 does not communicate, while Encoder 2's maximum rate can coexist with a non-zero rate for Encoder 1.

In contrast, by Corollary 1, for sufficiently high power P, both encoders can communicate with the decoder at their respective maximum rates. This is verified by Fig. 3, where

TABLE I
Phases of $\boldsymbol{H}_{ri}$ and $\boldsymbol{h}_d$ used for the numerical examples

Figure	$\angle \boldsymbol{H}_{ri}$ [rad]	$\angle \boldsymbol{h}_d$ [rad]
2	$\begin{pmatrix} 1.11 & 0.71 & 2.92 & -2.29 \\ 2.52 & -0.72 & 2.21 & 2.1 \end{pmatrix}$	$\begin{pmatrix} 3.11 \\ 1.39 \end{pmatrix}$
3	$\begin{pmatrix} -2.63 & -1.22 & -2.92 & -1.52 \\ 1.85 & 0.36 & -0.87 & -2.59 \end{pmatrix}$	$\begin{pmatrix} 2.82 \\ 2.32 \end{pmatrix}$

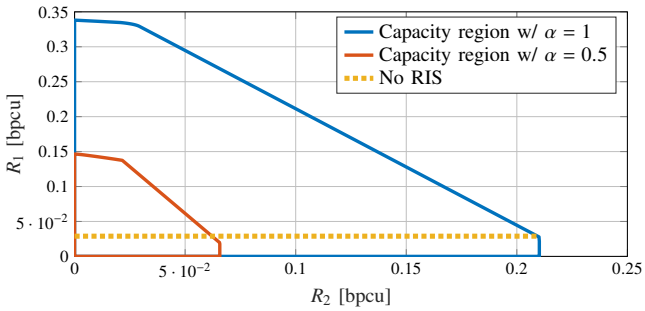

Fig. 2. Capacity region for $P = -20$ dB, $N = 2$, $K = 4$, $A = 2$, $m = 2$, and BPSK input constellation. The dashed line illustrates the capacity of Encoder 1 for a channel with no RIS.

we plot the capacity region for an average power constraint of $P = 40$ dB, $N = 2$ receiver antennas, $K = 4$ RIS elements, $A = 2$ available phase shifts, a symbol-to-RIS control rate $m = 1$, input constellation given by 4-ASK, i.e., $\mathcal{S} = \{\sigma, 3\sigma, 5\sigma, 7\sigma\}$ with $\sigma = 1/\sqrt{21}$, and a path-loss ratio of $\alpha = 1$. Although Encoder 1 does not gain from the existence of the RIS in the high-power regime, the RIS enables MU communication with a single transmitter in a manner that resembles the single-RF multiple-input multiple-output (MIMO) system [19], [25].

V. Conclusion

In this work, we have studied the finite-input capacity region of an RIS-aided MU communication system, in which the RIS is not used solely for increasing the rate of an active encoder, but also for enabling communication for a secondary passive encoder. The fundamental trade-offs between the rates of the two encoders were characterized. It was shown that, for sufficiently high power, both users can communicate at their respective maximum rates. Furthermore, in the low-power regime, the maximum rate for the active encoder is achieved if and only if the passive encoder does not communicate, while the passive encoder's maximum rate can coexist with a non-zero rate for the active encoder. Finally, time-sharing was demonstrated to be suboptimal.

Appendix

A. Proof of Proposition 1

The model (3) can be viewed as a MAC with inputs $(\mathbf{s}, \boldsymbol{\theta})$ and output $\mathbf{y}$. Therefore, it follows from the capacity region of the MAC [26, Thm. 4.2] that $\mathcal{C}(\boldsymbol{H}_{ri}, \boldsymbol{h}_d)$ is the convex hull of the union of regions $\tilde{\mathcal{R}}(p_{\mathbf{s}}, p_{\boldsymbol{\theta}}, \boldsymbol{H}_{ri}, \boldsymbol{h}_d)$ over all input distributions $p_{\mathbf{s}}(\boldsymbol{s})$ and $p_{\boldsymbol{\theta}}(\boldsymbol{\theta})$ such that $\mathbb{E}[\mathbf{s}^*\mathbf{s}] \le m$, where $\tilde{\mathcal{R}}(p_{\mathbf{s}}, p_{\boldsymbol{\theta}}, \boldsymbol{H}_{ri}, \boldsymbol{h}_d)$ is the set of rate pairs $(R_1(\boldsymbol{H}_{ri}, \boldsymbol{h}_d), R_2(\boldsymbol{H}_{ri}, \boldsymbol{h}_d))$ such that inequalities

$$R_1(\boldsymbol{H}_{ri}, \boldsymbol{h}_d) \le \frac{1}{m} I(\mathbf{s}; \mathbf{y}|\boldsymbol{\theta}), \quad R_2(\boldsymbol{H}_{ri}, \boldsymbol{h}_d) \le \frac{1}{m} I(\boldsymbol{\theta}; \mathbf{y}|\mathbf{s}), \tag{17a}$$

$$\text{and } R_1(\boldsymbol{H}_{ri}, \boldsymbol{h}_d) + R_2(\boldsymbol{H}_{ri}, \boldsymbol{h}_d) \le \frac{1}{m} I(\mathbf{s}, \boldsymbol{\theta}; \mathbf{y}) \tag{17b}$$

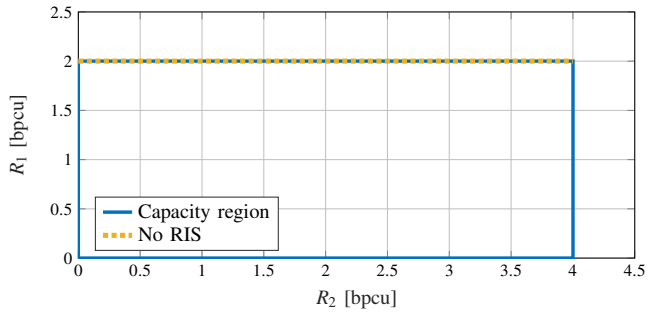

Fig. 3. Capacity region for $P = 40$ dB, $N = 2$, $K = 4$, $A = 2$, $m = 1$, and 4-ASK input constellation. The dashed line illustrates the capacity of Encoder 1 for a channel with no RIS.

hold. Since inputs $\mathbf{s}$ and $\boldsymbol{\theta}$ are selected from finite sets, the mutual information $I(\mathbf{s};\mathbf{y}|\boldsymbol{\theta})$ in (17) can be written as (see, e.g., [19, App. A])

$$I(\mathbf{s};\mathbf{y}|\boldsymbol{\theta}) = -NM\log_2(e) - \int_{\mathbb{C}^{Nm\times 1}} p_{\mathbf{z}}(\boldsymbol{z}) \sum_{\boldsymbol{s}_1\in\mathcal{S}^{m\times 1}} p_{\mathbf{s}}(\boldsymbol{s}_1) \sum_{\boldsymbol{\theta}_1\in\mathcal{A}^{K\times 1}} p_{\boldsymbol{\theta}}(\boldsymbol{\theta}_1) \log_2\left(\sum_{\boldsymbol{s}_2\in\mathcal{S}^{m\times 1}} p_{\mathbf{s}}(\boldsymbol{s}_2) e^{u_1}\right) \mathrm{d}\boldsymbol{z} \quad (18)$$

with $\mathbf{z} \sim \mathcal{CN}(\mathbf{0}, \boldsymbol{I}_{Nm})$ and where we have defined the scalar

$$u_1 \triangleq -\left\| \boldsymbol{z} + \sqrt{P}\left(\boldsymbol{H}_{ri} e^{j\boldsymbol{\theta}_1} + \boldsymbol{h}_d\right)^{m\otimes} (\boldsymbol{s}_1 - \boldsymbol{s}_2) \right\|^2. \quad (19)$$

By applying the conditional CGF definition in (4) to (18), we get

$$I(\mathbf{s};\mathbf{y}|\boldsymbol{\theta}) = -Nm\log_2(e) - \kappa(\mathrm{u}_1|\mathbf{s}_1, \boldsymbol{\theta}_1, \mathbf{z}). \quad (20)$$

Similarly, we also have

$$I(\boldsymbol{\theta};\mathbf{y}|\mathbf{s}) = -Nm\log_2(e) - \kappa(\mathrm{u}_2|\mathbf{s}_1, \boldsymbol{\theta}_1, \mathbf{z}), \quad (21a)$$
$$I(\mathbf{s},\boldsymbol{\theta};\mathbf{y}) = -Nm\log_2(e) - \kappa(\mathrm{u}_3|\mathbf{s}_1, \boldsymbol{\theta}_1, \mathbf{z}). \quad (21b)$$

Therefore, the region $\tilde{\mathcal{R}}(p_{\mathbf{s}}, p_{\boldsymbol{\theta}}, \boldsymbol{H}_{ri}, \boldsymbol{h}_d)$ in (17) is identical to the region $\mathcal{R}(p_{\mathbf{s}}, p_{\boldsymbol{\theta}}, \boldsymbol{H}_{ri}, \boldsymbol{h}_d)$ in (5).

B. Proof of Corollary 1

The inclusion $\mathcal{C}(\boldsymbol{H}_{ri}, \boldsymbol{h}_d) \subseteq \overline{\mathcal{C}}$ is trivial since, for all input distributions $p_{\mathbf{s}}(\boldsymbol{s})$ and $p_{\boldsymbol{\theta}}(\boldsymbol{\theta})$ with $\boldsymbol{s} \in \mathcal{S}^{m\times 1}$ and $\boldsymbol{\theta} \in \mathcal{A}^{K\times 1}$ we have $H(\mathbf{s}) \le m\log_2(S)$ and $H(\boldsymbol{\theta}) \le K\log_2(A)$. In addition, in the high-power regime, we have the limits

$$I(\mathbf{s};\mathbf{y}|\boldsymbol{\theta}) \xrightarrow[P\to\infty]{} H(\mathbf{s}) \le m\log_2(S), \quad (22a)$$
$$I(\boldsymbol{\theta};\mathbf{y}|\mathbf{s}) \xrightarrow[P\to\infty]{} H(\boldsymbol{\theta}) \le K\log_2(A), \quad (22b)$$

where equality is achieved for a uniform distributions $p_{\mathbf{s}}(\boldsymbol{s})$ and $p_{\boldsymbol{\theta}}(\boldsymbol{\theta})$. Next, note that the noiseless received signal $\mathbf{y}(t) - \mathbf{z}(t)$ in (3) takes values from a discrete set. Furthermore, since channel matrix $\mathbf{H}_{ri}$ and channel vector $\mathbf{h}_d$ are drawn from a continuous distribution, almost surely, for all $t \in [n/m]$, there exist unique inputs $\hat{\boldsymbol{s}}(t) \in \mathcal{S}^{m\times 1}$ and $\hat{\boldsymbol{\theta}}(t) \in \mathcal{A}^{K\times 1}$ such that (see, e.g., [27])

$$\mathbf{y}(t) - \mathbf{z}(t) = \sqrt{P}\left(\boldsymbol{H}_{ri} e^{j\hat{\boldsymbol{\theta}}(t)} + \boldsymbol{h}_d\right)^{m\otimes} \hat{\boldsymbol{s}}(t). \quad (23)$$

Therefore, for all input distributions $p_{\mathbf{s}}(\boldsymbol{s})$ and $p_{\boldsymbol{\theta}}(\boldsymbol{\theta})$, the transmitted signal $\mathbf{s}(t)$ and reflection pattern $\boldsymbol{\theta}(t)$ can be correctly jointly decoded in the high-power regime, i.e., we have the limit

$$I(\mathbf{s},\boldsymbol{\theta};\mathbf{y}) \xrightarrow[P\to\infty]{} H(\mathbf{s}) + H(\boldsymbol{\theta}) \le m\log_2(S) + K\log_2(A). \quad (24)$$

Let $\left(R_1^u(\boldsymbol{H}_{ri}, \boldsymbol{h}_d), R_2^u(\boldsymbol{H}_{ri}, \boldsymbol{h}_d)\right) \in \mathcal{C}(\boldsymbol{H}_{ri}, \boldsymbol{h}_d)$ be the rate pair achieved using uniform distributions $p_{\mathbf{s}}(\boldsymbol{s})$ and $p_{\boldsymbol{\theta}}(\boldsymbol{\theta})$. It hence follows from the region in (17) and limits (22) and (24) that, almost surely, we have the limits

$$\lim_{P\to\infty} R_1^u(\boldsymbol{H}_{ri}, \boldsymbol{h}_d) = \log_2(S), \quad (25a)$$
$$\lim_{P\to\infty} R_2^u(\boldsymbol{H}_{ri}, \boldsymbol{h}_d) = \frac{K}{m}\log_2(A). \quad (25b)$$

C. Proof of Proposition 2

For input distributions $p_{\mathrm{s}}(s)$ and $p_{\boldsymbol{\theta}}(\boldsymbol{\theta})$, let functions $\tilde{R}_\ell(P, \boldsymbol{h}_{ri}, h_d)$, $\ell \in \{1,2,3\}$, be defined as

$$\tilde{R}_\ell(P, \boldsymbol{h}_{ri}, h_d) \triangleq -\log_2(e) - \kappa(\mathrm{u}_\ell|\mathrm{s}_1, \boldsymbol{\theta}_1, \mathrm{z}), \quad (26)$$

where $\kappa(\mathrm{u}_\ell|\mathrm{s}_1, \boldsymbol{\theta}_1, \mathrm{z})$ are the conditional CGFs in Proposition 1 for the special case in which $N = m = 1$. By calculating the derivative of $\tilde{R}_\ell(P, \boldsymbol{h}_{ri}, h_d)$ with respect to the power P and taking the limit $P \to 0$, we get

$$\lim_{P\to 0} \frac{\partial \tilde{R}_\ell(P, \boldsymbol{h}_{ri}, h_d)}{\partial P} = \frac{\mathbb{E}[\underline{\mathrm{u}}_\ell]}{\ln(2)}, \quad (27)$$

where random variables $\underline{\mathrm{u}}_\ell$ are defined in (12). Therefore, it follows from Proposition 1 that the normalized rate pairs $(r_1(\boldsymbol{h}_{ri}, h_d), r_2(\boldsymbol{h}_{ri}, h_d))$ satisfy

$$r_\ell(\boldsymbol{h}_{ri}, h_d) = \lim_{P\to 0} \frac{R_\ell(\boldsymbol{h}_{ri}, h_d)}{P} \le \lim_{P\to 0} \frac{\tilde{R}_\ell(P, \boldsymbol{h}_{ri}, h_d)}{P} = \lim_{P\to 0} \frac{\partial \tilde{R}_\ell(P, \boldsymbol{h}_{ri}, h_d)}{\partial P} = \frac{\mathbb{E}[\underline{\mathrm{u}}_\ell]}{\ln(2)}, \quad \ell \in \{1,2\}, \quad (28)$$

and similarly we have

$$r_1(\boldsymbol{h}_{ri}, h_d) + r_2(\boldsymbol{h}_{ri}, h_d) \le \frac{\mathbb{E}[\underline{\mathrm{u}}_3]}{\ln(2)}. \quad (29)$$

D. Proof of Corollary 2

Since s_1, s_2, and $\boldsymbol{\theta}_1$ in Proposition 2 are all independent, we have

$$\mathbb{E}[\underline{\mathrm{u}}_1] = \mathbb{E}\left[\left|\left(\boldsymbol{h}_{ri}^{\mathsf{T}} e^{j\boldsymbol{\theta}_1} + h_d\right)(\mathrm{s}_1 - \mathrm{s}_2)\right|^2\right] \quad (30)$$
$$= \mathbb{E}\left[\left|\boldsymbol{h}_{ri}^{\mathsf{T}} e^{j\boldsymbol{\theta}_1} + h_d\right|^2\right] \mathbb{E}\left[|\mathrm{s}_1 - \mathrm{s}_2|^2\right] \le 2\left|\boldsymbol{h}_{ri}^{\mathsf{T}} e^{j\tilde{\boldsymbol{\theta}}} + h_d\right|^2.$$

Similarly, we have the upper bounds

$$\mathbb{E}[\underline{\mathrm{u}}_2] \le 2\|\boldsymbol{h}_{ri}\|^2, \quad (31a)$$
$$\mathbb{E}[\underline{\mathrm{u}}_3] \le 2\left|\boldsymbol{h}_{ri}^{\mathsf{T}} e^{j\tilde{\boldsymbol{\theta}}} + h_d\right|^2. \quad (31b)$$

Equality in (30) and (31b) is achieved for fixed RIS reflection pattern $\boldsymbol{\theta} = \tilde{\boldsymbol{\theta}}$ with probability one and uniform input distribution $p_{\mathrm{s}}(s) = 1/S$. Furthermore, since the upper bounds in (30) and (31b) are equal, Encoder 1 can achieve the maximum normalized rate if and only if $\boldsymbol{\theta} = \tilde{\boldsymbol{\theta}}$ with probability one. In contrast, equality in (31a) is achieved for uniform phase-shift distribution $p_{\boldsymbol{\theta}}(\boldsymbol{\theta}) = 1/A^K$ and any input distribution $p_{\mathrm{s}}(s)$ for which $\mathbb{E}[|\mathrm{s}|^2] = 1$. That is, Encoder 2 can achieve the maximum normalized rate, while Encoder 1 transmits at a positive normalized rate.

REFERENCES

[1] M. Di Renzo, A. Zappone, M. Debbah, M.-S. Alouini, C. Yuen, J. de Rosny, and S. Tretyakov, "Smart radio environments empowered by reconfigurable intelligent surfaces: How it works, state of research, and the road ahead," *IEEE J. Sel. Areas Commun.*, vol. 38, no. 11, pp. 2450–2525, 2020.

[2] M. Di Renzo, K. Ntontin, J. Song, F. H. Danufane, X. Qian, F. Lazarakis, J. De Rosny, D.-T. Phan-Huy, O. Simeone, R. Zhang, M. Debbah, G. Lerosey, M. Fink, S. Tretyakov, and S. Shamai, "Reconfigurable intelligent surfaces vs. relaying: Differences, similarities, and performance comparison," *IEEE Open Journal of the Communications Society*, vol. 1, pp. 798–807, 2020.

[3] Q. Wu and R. Zhang, "Towards smart and reconfigurable environment: Intelligent reflecting surface aided wireless network," *IEEE Commun. Mag.*, vol. 58, no. 1, pp. 106–112, 2020.

[4] Y. Liu, X. Liu, X. Mu, T. Hou, J. Xu, Z. Qin, M. Di Renzo, and N. Al-Dhahir, "Reconfigurable intelligent surfaces: Principles and opportunities," *arXiv preprint arXiv:2007.03435*, 2020.

[5] M. Di Renzo, M. Debbah, D.-T. Phan-Huy, A. Zappone, M.-S. Alouini, C. Yuen, V. Sciancalepore, G. C. Alexandropoulos, J. Hoydis, H. Gacanin, J. de Rosny, A. Bounceu, G. Lerosey, and M. Fink, "Smart radio environments empowered by AI reconfigurable meta-surfaces: An idea whose time has come," *EURASIP J. Wireless Commun. Netw.*, pp. 1–20, 2019.

[6] X. Yuan, Y. J. Angela Zhang, Y. Shi, W. Yan, and H. Liu, "Reconfigurable-intelligent-surface empowered wireless communications: Challenges and opportunities," *IEEE Wireless Communications*, pp. 1–8, 2021.

[7] Q. Wu, S. Zhang, B. Zheng, C. You, and R. Zhang, "Intelligent reflecting surface aided wireless communications: A tutorial," *IEEE Trans. Commun.*, 2021.

[8] H. Guo, Y. C. Liang, J. Chen, and E. G. Larsson, "Weighted sum-rate maximization for intelligent reflecting surface enhanced wireless networks," in *Proc. IEEE Global Conf. Communications (GLOBECOM)*, 2019, pp. 1–6.

[9] H. Zhang, B. Di, Z. Han, H. V. Poor, and L. Song, "Reconfigurable intelligent surface assisted multi-user communications: How many reflective elements do we need?" *IEEE Wireless Commun. Lett.*, 2021.

[10] A. Abrardo, D. Dardari, and M. Di Renzo, "Intelligent reflecting surfaces: Sum-rate optimization based on statistical CSI," *arXiv preprint arXiv:2012.10679*, 2020.

[11] X. Mu, Y. Liu, L. Guo, J. Lin, and R. Schober, "Joint deployment and multiple access design for intelligent reflecting surface assisted networks," *arXiv preprint arXiv:2005.11544*, 2020.

[12] C. Huang, A. Zappone, G. C. Alexandropoulos, M. Debbah, and C. Yuen, "Reconfigurable intelligent surfaces for energy efficiency in wireless communication," *IEEE Trans. Wireless Commun.*, vol. 18, no. 8, pp. 4157–4170, 2019.

[13] H. Han, J. Zhao, D. Niyato, M. D. Renzo, and Q. Pham, "Intelligent reflecting surface aided network: Power control for physical-layer broadcasting," in *Proc. IEEE Int. Conf. Communications (ICC)*, 2020, pp. 1–7.

[14] J. Zhang, H. Du, Q. Sun, D. W. K. Ng, and B. Ai, "Physical layer security enhancement with reconfigurable intelligent surface-aided networks," *arXiv preprint arXiv:2012.00269*, 2020.

[15] G. Zhou, C. Pan, H. Ren, K. Wang, and M. Di Renzo, "Fairness-oriented multiple RISs-aided MmWave transmission: Stochastic optimization approaches," *arXiv preprint arXiv:2012.06103*, 2020.

[16] L. Yang, F. Meng, M. O. Hasna, and E. Basar, "A novel RIS-assisted modulation scheme," *IEEE Wireless Commun. Lett.*, 2021.

[17] S. R. B. Pillai, "On the capacity of multiplicative multiple access channels with awgn," in *Proc. IEEE Inform. Theory Workshop (ITW)*, 2011, pp. 452–456.

[18] W. Liu, Y. Liang, Y. Li, and B. Vucetic, "Backscatter multiplicative multiple-access systems: Fundamental limits and practical design," *IEEE Trans. Wireless Commun.*, vol. 17, no. 9, pp. 5713–5728, 2018.

[19] R. Karasik, O. Simeone, M. Di Renzo, and S. Shamai, "Adaptive coding and channel shaping through reconfigurable intelligent surfaces: An information-theoretic analysis," *arXiv preprint arXiv:2012.00407*, 2020.

[20] Y. Wu, C. Xiao, Z. Ding, X. Gao, and S. Jin, "A survey on MIMO transmission with finite input signals: Technical challenges, advances, and future trends," *Proceedings of the IEEE*, vol. 106, no. 10, pp. 1779–1833, 2018.

[21] S. Verdu, "Spectral efficiency in the wideband regime," *IEEE Trans. Inf. Theory*, vol. 48, no. 6, pp. 1319–1343, Jun 2002.

[22] J. L. Massey, "All signal sets centered about the origin are optimal at low energy-to-noise ratios on the awgn channel," in *Proc. IEEE Int. Symp. Inform. Theory (ISIT)*, 1976, pp. 80–81.

[23] A. Lapidoth and S. Shamai, "Fading channels: how perfect need "perfect side information" be?" *IEEE Trans. Inf. Theory*, vol. 48, no. 5, pp. 1118–1134, 2002.

[24] G. Caire, D. Tuninetti, and S. Verdu, "Suboptimality of TDMA in the low-power regime," *IEEE Trans. Inf. Theory*, vol. 50, no. 4, pp. 608–620, April 2004.

[25] Q. Li, M. Wen, and M. Di Renzo, "Single-RF MIMO: From spatial modulation to metasurface-based modulation," *arXiv preprint arXiv:2009.00789*, 2020.

[26] A. El Gamal and Y.-H. Kim, *Network information theory*. Cambridge university press, 2011.

[27] A. S. Motahari, S. Oveis-Gharan, M. A. Maddah-Ali, and A. K. Khandani, "Real interference alignment: Exploiting the potential of single antenna systems," *IEEE Trans. Inf. Theory*, vol. 60, no. 8, pp. 4799–4810, Aug. 2014.